UAV Positioning and RIS Partitioning for Connectivity of Uplink RIS-Assisted UAV Networks

Mohammed Saif and Shahrokh Valaee
Department of Electrical and Computer Engineering, University of Toronto, Toronto, Canada
Email: mohammed.saif@utoronto.ca, valaee@ece.utoronto.ca

***Abstract*—In this paper, we present a new approach for unmanned aerial vehicle (UAV) positioning and reconfigurable intelligent surface (RIS) partitioning to enhancing connectivity of uplink RIS-assisted UAV networks. To achieve this, our approach optimizes UAV positions and RIS partitioning to maximize network connectivity characterized by its Fiedler value. Meanwhile, it maintains particular signal-to-noise ratio (SNR) constraint to user equipments (UEs), featured by RIS partitioning and UAV reliability. The network connectivity optimization problem is formulated using the Fiedler value subject to RIS elements allocation and SNR constraints. This problem is a computationally expensive combinatorial optimization, necessitating an efficient iterative approach. In particular, given UAVs positions, we derive a closed-form solution for RIS partitioning, with each partition tailored to optimize SNR for individual UAV. For the given RIS partitioning, we then show that the problem of UAV positioning can be formulated as a low complexity semi-definite programming (SDP) optimization problem, which can be solved using off-the-shelf CVX solvers. Our simulations show the potential gain of UAV positioning and RIS partitioning compared to the benchmark schemes from the literature.**

***Index Terms*—Network connectivity, RIS-assisted UAV communications, RIS partitioning, SDP optimization.**

I. Introduction

Optimizing the locations of unmanned aerial vehicles (UAVs) is essential for a wide range of applications, including extending network coverage, enhancing connectivity and resiliency, and improving localization and tracking [1]–[3]. Additionally, the flexible deployment of UAVs allows the establishment of line-of-sight (LoS) communications to geographically distant user equipments (UEs), enabling a large number of UEs to connect to the network and reducing the probability of unconnected UEs. Since UAVs are prone to failure, because of limited energy, deploying more UAVs is not preferred. This causes network disintegration and severely disrupts information flow of UEs.

Reconfigurable intelligent surfaces (RISs) have emerged as a low-cost solution for controlling the wireless environment, with significant potential for improving network connectivity and extending service coverage. By manipulating the propagation environment, RISs can significantly enhance localization [4], [5], energy efficiency [6], coverage [7], and network connectivity [8]. RIS composes of configurable elements with the ability to re-design the channel by changing the phase of the incident signals. From a connectivity perspective, RISs can introduce additional links to networks and significantly enhance connectivity. RISs can also compromise UAV failures—measured by the removal of UAV nodes from the network—by redirecting UE signals to reliable UAVs, thereby maintaining network integrity.

Most studies on maximizing network connectivity have primarily focused on utilizing UAVs [3], relays [9], or sensors [10] in different systems. The authors of [3] maximize network connectivity, modeled by the Fiedler value (i.e., the second smallest eigenvalue of the Laplacian graph network [11]), by optimizing UAV positioning in small-cell systems. The works [9], [10] consider optimizing the placement of relays and sensors for connectivity maximization and network repair maintenance. On the other hand, the work [8] improves network connectivity and resiliency of cell-free networks using RIS deployment.

Recently, the convergence of RIS and UAV technologies has been leveraged for enhancing key performance metrics, including physical layer security [12] and connectivity [13], [14]. Integrating RIS technology with UAVs introduces numerous optimization challenges, such as UAV positioning, UE-RIS-UAV link selection, and RIS phase design [7]. The recent works [13], [14] improve connectivity of RIS-assisted UAV networks using RIS deployment, with the optimization of UE-RIS-UAV link selection and RIS phase design only. Both works propose to generate one UE-RIS-UAV link from each RIS, ignoring the efficient use of RIS that could be utilized to generate multiple links in the network. In addition, they do not consider optimizing UAV location to further improve network connectivity and coverage.

Motivated by the aforementioned studies, this work delves into the RIS partitioning and UAV positioning approach in RIS-assisted UAV networks, wherein the RIS elements are optimally partitioned and assigned to the corresponding UAVs, fulfilling their signal-to-noise ratio (SNR) conditions. The main findings of this paper can be summarized as follows. The network connectivity optimization problem is formulated using the Fiedler value subject to RIS elements allocation and SNR constraints. To tackle this problem, for given UAVs positions, we derive a closed-form solution for RIS partitioning. For the given RIS partitioning, we then show that the problem of UAV positioning can be formulated as a low complexity semi-definite programming (SDP) optimization problem, which can be solved using off-the-shelf CVX solvers. Our simulations show the potential gain of the proposed iterative solution compared to the benchmark schemes from the literature.

This work was supported in part by funding from the Innovation for Defence Excellence and Security (IDEaS) program from the Department of National Defence (DND) of Canada.

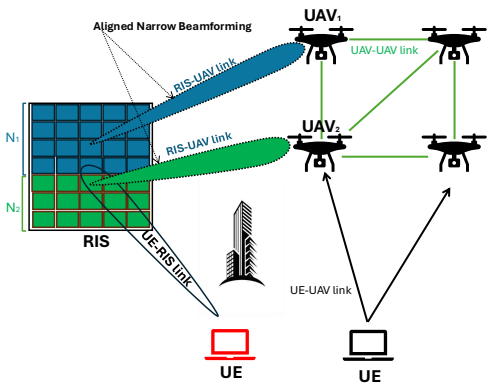

Fig. 1. System model for an uplink-RIS-assisted UAV network.

II. System Model

A. Network Model

Consider an uplink-RIS-assisted UAV model as shown in Fig. 1, where a set of single-antenna UEs, denoted by $\mathcal{M} = \{1, 2, \ldots, M\}$, transmit signals to a set of single-antenna UAVs, denoted by $\mathcal{K} = \{1, 2, \ldots, K\}$, with the aid of RIS comprising of N passive elements. In practice, direct links between the UEs and the UAVs might be blocked, and the RIS can aid in establishing reliable communication with the blocked UAVs. In addition, through positioning optimization, the UAVs aim to extend the service coverage area and serve the M UEs, which are in deep fade situation. Assuming that the channel state information (CSI) is available, the optimal RIS phase shifts are calculated and reported back to the RIS controller through dedicated feedback channels [12]. The model assumes that communications take place using orthogonal resources, such as frequency or time division duplexing, to prevent interference. In this setup, only one UE transmits at a time, while all other UEs remain idle during that period.

The RIS can reflect the signal of the transmitted UE to multiple UAVs through virtual partitioning representation; however, the RIS cannot be assigned to more than one UE at the same time [12]. The set of multiple UAVs that exploit the RIS is denoted as $\mathcal{K}_m$, which also represents the number of partitions in the RIS, i.e., $\mathcal{K}_m = \{\text{UAV}_1, \text{UAV}_2\}$ and $K_m = 2$ in Fig. 1. We represent the RIS elements' allocation portions $\boldsymbol{\alpha} = [\alpha_1, \ldots, \alpha_{K_m}]$ to denote the RIS portions that are allocated to UAV_k, $k \in \{1, \ldots, K_m\}$, respectively. The number of RIS elements designated for UAV_k is N_k, which can be presented as $N_k = \lceil \alpha_k N \rceil$. In Fig. 1, UAV_1 obtains a coherently aligned link from the designated RIS portion α_1 and a non-coherently aligned link from the remaining RIS portion α_2.

We model the uplink RIS-assisted UAV network using an undirected, weighted, simple finite graph $\mathcal{G}(\mathcal{V}, \mathcal{E})$, where $\mathcal{V} = \{v_1, \ldots, v_V\}$ is the set of vertices (nodes) and $\mathcal{E} = \{e_1, \ldots, e_E\}$ is the set of E edges connecting the nodes. For any edge l between two vertices v_i and $v_j \in \mathcal{V}$, the edge vector $\mathbf{a}_l \in \mathbf{R}^V$ is a vector of zeros except for its i-th and j-th elements, where $a_{l,i} = 1$ and $a_{l,j} = -1$, respectively. The graph's incidence matrix of $\mathbf{A} \in \mathbf{R}^{V \times E}$ is constructed as $\mathbf{A} = [\mathbf{a}_l, \ldots, \mathbf{a}_E]$. The Laplacian matrix of the graph, $\mathbf{L} \in R^{V \times V}$, is then given as follows [3]

$$\mathbf{L} = \mathbf{A}\ diag(\mathbf{w})\ \mathbf{A}^T = \sum_{l=1}^{E} w_l \mathbf{a}_l \mathbf{a}_l^T, \tag{1}$$

where $\mathbf{w} \in [\mathbb{R}^+]^E$ denotes the $E \times 1$ weighting vector coefficients for the E edges and is given by $\mathbf{w} = [w_1, w_2, \ldots, w_E]$. The weights of the edges are based on their corresponding SNRs that are modeled as in [3], while the connections of the edges are based on SNR thresholds, i.e., γ_0^{UE} and γ_0^{UAV} for $\text{UE} \rightarrow \text{UAV}_k$ and $\text{UAV}_k \rightarrow \text{UAV}_{k'}$, respectively. The Laplacian matrix $\mathbf{L}$ is a positive semi-definite matrix, i.e., $\mathbf{L} \geq 1$. Its second smallest eigenvalue, denoted by $\lambda_2(\mathbf{L})$, is known as the Fiedler value. A higher Fiedler value indicates stronger overall network connectivity, while $\lambda_2(\mathbf{L}) = 0$ implies that the graph is disconnected [11].

The deployment of UAV positioning and RIS partitioning can create more links, thereby a new graph $\mathcal{G}'(\mathcal{V}, \mathcal{E}')$ is built with the same number of V nodes and a larger set of edges denoted by $\mathcal{E}'$ with $\mathcal{E}' = \mathcal{E} \cup \mathcal{E}_{new}$, where $\mathcal{E}_{new}$ is the new edges for the $\text{UE} \rightarrow \text{UAV}_{k \in \mathcal{K}_m}$ links. In particular, such deployment has an impact on relaying information from UEs to UAVs and extends the coverage, creating additional $E' - E$ edges to the original network. By comparing the network graphs before and after the deployment, the connectivity improvement can be quantified by evaluating the change in the Fiedler value. Specifically, the gain is observed when $\lambda_2(\mathbf{L}') \geq \lambda_2(\mathbf{L})$, where $\mathbf{L}'$ represents the Laplacian matrix of the updated graph $\mathcal{G}'(\mathcal{V}, \mathcal{E}')$.

Each UAV has a different impact on network connectivity when it is removed from the graph along with its connected edges to other nodes. For this, we measure the reliability of $\text{UAV}_{k \in \mathcal{K}m}$ based on this impact on network connectivity, defined as $\mathcal{R}_k = \lambda_2(\mathcal{G}_{-k})$, where $\mathcal{G}_{-k}$ is the subgraph resulting from removing UAV_k and all its adjacent edges to other nodes in $\mathcal{G}$.

B. Channel Model and SNR Formulation

All channels of UE-UAV, UE-RIS, and RIS-UAV are considered to be quasi-static with flat-fading and follow the Nakagami-f fading model [12]. Let $(\mathbf{g}^{\text{UR}}, \beta^{\text{UR}})$ and $(\mathbf{g}_k^{\text{RK}}, \beta_k^{\text{RK}})$ represent the small-scale fading coefficients and path-losses for the $\text{UE} \rightarrow \text{RIS}$ and $\text{RIS} \rightarrow \text{UAV}_k$ channels, respectively. Here, $\mathbf{g}^{\text{UR}} = [g_n^{\text{UR}}, \ldots, g_N^{\text{UR}}]$ and $\mathbf{g}_k^{\text{RK}} = [g_{n,k}^{\text{RK}}, \ldots, g_{N,k}^{\text{RK}}]$. Therefore, we consider the channel from the UE to UAV_k over the n-th RIS element as $g_{n,k}^{\text{URK}} = g_n^{\text{UR}} g_{n,k}^{\text{RK}}$, where $g_n^{\text{UR}} = |g_n^{\text{UR}}| e^{-j\phi_n}$ denotes the channel coefficient between the UE and the n-th RIS element, while $g_{n,k}^{\text{RK}} = |g_{n,k}^{\text{RK}}| e^{-j\psi_{n,k}}$ is the channel coefficient between the n-th RIS element and UAV_k; $|g_n^{\text{UR}}|$ and $|g_{n,k}^{\text{RK}}|$ are the channel amplitudes, while ϕ_n and $\psi_{n,k}$ are the channel phases. Moreover, for the direct links between the UE and the UAVs, let g_k^{UK} and β_k^{UK} denote the small-scale fading coefficient and path-loss for the $\text{UE} \rightarrow \text{UAV}_k$ channel, respectively.

To quantify the coverage of the UAVs to both the RIS and the UE, we utilize the instantaneous signal-to-noise ratio (SNR). This metric is suitable for the access network, as the UAVs establish single-hop links with the UEs, making the instantaneous SNR a reliable indicator of coverage quality [3]. Thus, the SNR at UAV$_k$ can be expressed as[1]

$$\begin{aligned}\mathrm{SNR}_k(\boldsymbol{\alpha}) &= \frac{p\Big[\underbrace{\sqrt{\beta^{\mathrm{UK}}}g_k^{\mathrm{UK}}}_{\textbf{direct link}} + \underbrace{\sqrt{\beta^{\mathrm{UR}}\beta_k^{\mathrm{RK}}}\sum_{n=1}^{N_k} g_{n,k}^{\mathrm{URK}}e^{j\theta_n}}_{\textbf{aligned phase}}\Big]^2}{N_0} \\ &\overset{(a)}{=} \frac{p\Big[\sqrt{\beta^{\mathrm{UK}}}g_k^{\mathrm{UK}} + \sqrt{\beta^{\mathrm{UR}}\beta_k^{\mathrm{RK}}}\alpha_k\sum_{n=1}^{N}|g_n^{\mathrm{UR}}||g_{n,k}^{\mathrm{RK}}|\Big]^2}{N_0} \\ &\overset{(b)}{=} \frac{p\Big[\sqrt{\beta^{\mathrm{UK}}}g_k^{\mathrm{UK}} + \sqrt{\beta^{\mathrm{UR}}\beta_k^{\mathrm{RK}}}\alpha_k Q\Big]^2}{N_0},\end{aligned} \tag{2}$$

where N_0 is the additive white Gaussian noise (AWGN), p is the transmit power of the transmitting UE, $\overset{(a)}{=}$ comes from (i) $\sum_{n=1}^{N_k}(.) = \sum_{n=1}^{\lceil \alpha_k N\rceil}(.) = \alpha_k\sum_{n=1}^{N}(.)$ and (ii) $g_{n,k}^{\mathrm{URK}}e^{j\theta_n} = |g_n^{\mathrm{UR}}||g_{n,k}^{\mathrm{RK}}|e^{j(\theta_n-\phi_n-\psi_{n,k})} = |g_n^{\mathrm{UR}}||g_{n,k}^{\mathrm{RK}}|$; i.e., for the n-th RIS element, given ϕ_n and $\psi_{n,k}$, the RIS's controller can perfectly align θ_n with ϕ_n and $\psi_{n,j}$ to nullify their effect, and $\overset{(b)}{=}$ comes from $Q = \sum_{n=1}^{N}|g_n^{\mathrm{UR}}||g_{n,k}^{\mathrm{RK}}|$ which is the N-element double-Nakagami$-f$ that is independent and identically distributed (i.i.d.) random variable (RV) with parameters f_1, f_2, Ω_1, and Ω_2; the distribution of the product of two RVs following the Nakagami$-f$ distribution with the probability density function (PDF) is given in [12].

III. Problem Formulation

To fully demonstrate the effectiveness of integrating RIS technology with UAVs, it is essential to consider various degrees of freedom, such as UAV positioning, UE-RIS-UAV link selection, and RIS partitioning and phase shift design. The present paper focuses on two key degrees of freedom: UAV positioning and RIS partitioning, assuming that the UE-RIS-UAV links are preselected. Accordingly, we formulate an optimization problem that maximizes network connectivity by jointly optimizing UAV positioning and RIS partitioning, while ensuring that each selected UAV meets its SNR constraint. Let γ_{th} be the SNR threshold. Mathematically, the problem can be written as follows

$$\begin{aligned}\max_{\mathbf{0}\preceq\boldsymbol{\alpha}\preceq\mathbf{1},\boldsymbol{u}} \quad & \lambda_2(\mathbf{L}'(\boldsymbol{\alpha},\boldsymbol{u})) \\ \text{s. t.} \quad & \mathrm{SNR}_k(\boldsymbol{\alpha},\boldsymbol{u}) \geq \mathcal{R}_k\gamma_{\mathrm{th}}, \quad \forall k\in\{1,\ldots,K_m\}, \\ & \sum_{k=1}^{K}\alpha_k \leq 1,\end{aligned} \tag{3}$$

where $\boldsymbol{u} = [\boldsymbol{u}_1,\ldots,\boldsymbol{u}_{K_m}]$, where $\boldsymbol{u}_1$ is the 3×1 position vector in a Cartesian 3D coordinate system of UAV$_1$, and $\preceq$ is the pairwise inequality. The first constraint constitutes the SNR constraint on UAV$_k$, the second constraint ensures that the allocated portions do not exceed unity such that the total number of allocated RIS elements is not higher than the total number of RIS elements.

[1]Due to the complexity of the RIS partitioning optimization, the non-aligned phase term is removed from (2). Nonetheless, [12] shows that the impact of this term is minimal, as also confirmed by our numerical results.

Fig. 2. Diagram of the proposed solution.

IV. Proposed Solution

The problem in (3) is a computationally expensive combinatorial optimization. To tackle it over $\boldsymbol{\alpha}$ and $\boldsymbol{u}$, we decompose (3) into two subproblems and solve them iteratively. For given $\boldsymbol{u}$, we optimize $\lambda_2(\mathbf{L}'(\boldsymbol{\alpha}))$ by finding a closed-form solution of the RIS portions, denoted by $\boldsymbol{\alpha}^*$, that pushes the SNRs of UAV$_k$, $k\in\{1,\ldots,K_m\}$, to its maximum. By exploiting the closed-form RIS elements solution, we optimize the UAVs locations. The proposed solution is presented in Fig. 2.

A. RIS Partitioning Optimization

Maximizing network connectivity, characterized by the Fiedler value, involves optimizing the graph structure, specifically the selection of UEs and UAVs, as well as their link qualities. Given that the nodes (the UE and the UAV$_{k\in\mathcal{K}_m}$) are predetermined and network connectivity is a monotonically increasing function of the added links and their weights [11], this work equivalently maximizes the network connectivity by focusing on maximizing the SNR of the newly established UE $\xrightarrow{\text{RIS}}$ UAV$_{k\in\mathcal{K}_m}$ links.

For the given $\boldsymbol{u}$, we optimize $\boldsymbol{\alpha}$ to maximize the sum SNR of the new UE $\xrightarrow{\text{RIS}}$ UAV$_{k\in\mathcal{K}_m}$ links given SNR constraint based on UAV reliability and RIS elements. Thus, the subproblem for updating RIS partitioning is given by

$$\begin{aligned}\max_{\mathbf{0}\leq\boldsymbol{\alpha}\leq\mathbf{1}} \quad & \sum_{k=1}^{K_m}\mathrm{SNR}_k(\boldsymbol{\alpha}) \\ \text{s. t.} \quad & \mathrm{SNR}_k(\boldsymbol{\alpha}) \geq \mathcal{R}_k\gamma_{\mathrm{th}}, \quad \forall k\in\{1,\ldots,K_m\}, \\ & \sum_{k=1}^{K_m}\alpha_k \leq 1.\end{aligned} \tag{4}$$

The proceeding proposition provides the closed-form solution $\boldsymbol{\alpha}^*$ of (4).

Proposition 1. *The RIS partitioning that provides the maximized network connectivity via maximizing the sum SNR of the new UE $\xrightarrow{\text{RIS}}$ UAV$_{k\in\mathcal{K}_m}$ links is given by*

$$\alpha_k^* = \begin{cases}\sqrt{\frac{\mathcal{R}_k\gamma_{\mathrm{th}}N_0 - p\beta^{UK}}{p\beta^{UR}\beta_k^{RK}N^2 z}}, & \text{if } k\neq k^*, \\ 1-\sum_{k=1}^{K_m-1}\alpha_k^*, & \text{if } k=k^*.\end{cases} \tag{5}$$

Proof. Due to the complexity of obtaining $\boldsymbol{\alpha}$ directly from (2) and the first constraint of (4), which involves expansion and derivative, we first approximate the SNR expression in (2) by utilizing the expected values of

$\sqrt{\beta^{\text{UK}}}|g_k^{\text{UK}}|$ and $\alpha_k Q$. Specifically, the expectations can be evaluated as $\mathrm{E}\Big\{\Big[\sqrt{\beta^{\text{UK}}}|g_k^{\text{UK}}|\Big]^2\Big\} = \beta^{\text{UK}}$, since $g_k^{\text{UK}} \sim \mathcal{CN}(0,1)$, $\mathrm{E}\big\{|g_k^{\text{UK}}|^2\big\} = 1$; $\mathrm{E}\Big\{\Big[\sqrt{\beta^{\text{UR}}\beta_k^{\text{RK}}}\alpha_k Q\Big]^2\Big\} = \beta^{\text{UR}}\beta_k^{\text{RK}}\mathrm{E}\Big\{\Big[\alpha_k \sum_{n=1}^{N}|g_n^{\text{UR}}||g_{n,k}^{\text{RK}}|\Big]^2\Big\} = \beta^{\text{UR}}\beta_k^{\text{RK}}\alpha_k^2 N^2 \frac{1}{\tilde{f}\hat{f}}\frac{\Gamma(\tilde{f}+0.5)^2}{\Gamma(\tilde{f})^2}\frac{\Gamma(\hat{f}+0.5)^2}{\Gamma(\hat{f})^2} = \beta^{\text{UR}}\beta_k^{\text{RK}}\alpha_k^2 N^2 z$, where $z = \frac{1}{\tilde{f}\hat{f}}\frac{\Gamma(\tilde{f}+0.5)^2}{\Gamma(\tilde{f})^2}\frac{\Gamma(\hat{f}+0.5)^2}{\Gamma(\hat{f})^2}$, where $\Gamma(.)$ denotes the Gamma function. By substituting these values in (2), we have

$$\text{SNR}_k(\boldsymbol{\alpha}) = \frac{p[\beta^{\text{UK}} + \beta^{\text{UR}}\beta_k^{\text{RK}}\alpha_k^2 N^2 z]}{N_0}. \tag{6}$$

To maximize the sum SNR of UE $\xrightarrow{\text{RIS}}$ $\text{UAV}_{k\in\mathcal{K}_m}$ links while ensuring the constraints of (4), we assign portions of the RIS elements to the selected UAVs except for the UAV with the most reliability. Let k^* be the most reliable UAV, i.e., $k^* = \arg\max_{k\in\mathcal{K}_m}\{\mathcal{R}_k\}$. Thus, the SNRs of these $\text{UAV}_{k\in\mathcal{K}_m\setminus k^*}$ are just equal to their minimum required SNR. Lastly, the remaining elements of the RIS can be allocated to UAV_{k^*}, providing higher SNR for that UAV. Therefore, if we rewrite the first constraint in (4) using (6), for all the UAVs except UAV_{k^*}, as $\text{SNR}_k(\boldsymbol{\alpha}) = \frac{p[\beta^{\text{UK}}+\beta^{\text{UR}}\beta_k^{\text{RK}}\alpha_k^2 N^2 z]}{N_0} = \mathcal{R}_k\gamma_{\text{th}}$, we get (5). In addition, for UAV_{k^*}, $\alpha_{k^*}^* = 1 - \sum_{k=1}^{K_m-1}\alpha_k^*$, which completes the proof. ■

B. UAV Positioning Optimization

For the given $\boldsymbol{\alpha}^*$, the UAV positioning optimization is given by

$$\begin{aligned} \max_{\boldsymbol{u}} \quad & \lambda_2(\mathbf{L}'(\boldsymbol{u})) \\ \text{s. t.} \quad & \text{SNR}_k \geq \mathcal{R}_k\gamma_{\text{th}}, \quad \forall k \in \{1,\ldots,K_m\}. \end{aligned} \tag{7}$$

As explained in Section II, the Laplacian matrix $\lambda_2(\mathbf{L}'(\boldsymbol{u}))$ depends on UAV placement which determines the new links. This makes (7) a non-convex optimization problem, i.e., $\lambda_2(\mathbf{L}'(\boldsymbol{u}))$ is not a concave function. To address the non-concavity of $\lambda_2(\mathbf{L}'(\boldsymbol{u}))$, this paper leverages the structural properties of the graph Laplacian matrix to facilitate the optimization process.

Let $\boldsymbol{v} \in \mathbf{R}^V$ be the eigenvector corresponding to $\lambda_2(\mathbf{L})$, which has a unit norm $\|\boldsymbol{v}\|_2 = 1$ and is orthogonal to the all-ones vector $\mathbf{1}$, i.e., $\mathbf{1}^T\boldsymbol{v} = 0$, where $\mathbf{1}$ is $V \times 1$. Since $\mathbf{L}\boldsymbol{v} = \lambda_2\boldsymbol{v}$ [11], $\boldsymbol{v}^T\mathbf{L}\boldsymbol{v} = \lambda_2\boldsymbol{v}^T\boldsymbol{v} = \lambda_2$. Hence, $\lambda_2(\mathbf{L})$ can be expressed as the smallest eigenvalue that satisfies these conditions [3], [9], i.e.,

$$\lambda_2(\mathbf{L}) = \text{Inf}_{\boldsymbol{v}}\big\{\boldsymbol{v}^T\mathbf{L}\boldsymbol{v}, \quad \|\boldsymbol{v}\|_2 = 1, \quad \mathbf{1}^T\boldsymbol{v} = 0\big\}, \tag{8}$$

where Inf is the infimum of a set, which is also called the greatest lower bound (GLB). (8) can be expressed as a convex problem as

$$\begin{aligned} \lambda_2(\mathbf{L}) = \min_{\boldsymbol{v}\in\mathbf{R}^V} \quad & \boldsymbol{v}^T\mathbf{L}\boldsymbol{v} \\ \text{s. t.} \quad & \|\boldsymbol{v}\|_2 = 1, \ \mathbf{1}^T\boldsymbol{v} = 0. \end{aligned} \tag{9}$$

Additionally, there is indirect dependence between $\mathbf{L}'(\boldsymbol{u})$ and $\boldsymbol{u}$. To address this, we consider that UAVs are distributed within a $h\times h\times h$ volume. Additionally, the search space along the axes is uniformly quantized with a step size δ, generating J candidate search grids for each UAV. This simplifies $\mathbf{L}'(\boldsymbol{u})$ to be represented by

$$\mathbf{L}' = \mathbf{L} + \sum_{k=1}^{K_m}\sum_{j=1}^{J} x_j^{(k)}\mathbf{A}_j^{(k)}\text{diag}(w_j^{(k)})\mathbf{A}_j^{(k)}, \tag{10}$$

where $x_j^{(k)}$ is equal to one if UAV_k is located at the j-th grid point, otherwise $x_j^{(k)} = 0$. Moreover, $w_j^{(k)}$ and $\mathbf{A}_j^{(k)}$ are the weighting coefficient vectors and the incidence matrix when UAV_k is deployed at the j-th grid point, respectively.

Collecting $x_j^{(k)}$, for $k \in \{1,\ldots,K_m\}$ and $j \in \{1,\ldots,J\}$, in the $JK_m \times 1$ vector $\boldsymbol{x}$, (10) can be written as follows

$$\begin{aligned} \mathbf{L}' &= \mathbf{L} + \sum_{i=1}^{JK_m} x_i\mathbf{A}_i\text{diag}(w_i)\mathbf{A}_i \\ &= \mathbf{L} + (\boldsymbol{x}\otimes\mathbf{1}_V)\Delta, \end{aligned} \tag{11}$$

where $\Delta = \big[(\mathbf{A}_1\text{diag}(w_1)\mathbf{A}_1)^T, \ldots, (\mathbf{A}_{JK_m}\text{diag}(w_{JK_m})\mathbf{A}_{JK_m})^T\big]^T$. Note that since J is much larger than K_m, considering the vector $J \times 1$ instead of $JK_m \times 1$ is convenient to provide superior performance. Thus, the problem can be viewed as selecting the optimal K_m UAVs from a set of J candidate UAVs (i.e., J candidate grid points, with each UAV located at the center of its grid). Furthermore, by stacking the SNR levels between the transmitting UE, via the RIS, and UAV_k, which is placed at candidate positions in the search grid, into a $J \times 1$ vector denoted by $\boldsymbol{y}_k$, such that $\text{SNR}_k = \boldsymbol{x}^T\boldsymbol{y}_k$, the optimization problem in (7) can be written in terms of $\boldsymbol{x}$ rather than $\boldsymbol{u}$. Hence, the optimization problem in (7) can be written as follows

$$\begin{aligned} \max_{\boldsymbol{x}} \quad & \lambda_2(\mathbf{L}'(\boldsymbol{x})) \\ \text{s. t.} \quad & \boldsymbol{x}^T\boldsymbol{y}_k \geq \mathcal{R}_k\gamma_{\text{th}}, \quad \forall k \in \{1,\ldots,K_m\}, \\ & \mathbf{1}^T\boldsymbol{x} = K_m, \ \boldsymbol{x} \in \{0,1\}^J. \end{aligned} \tag{12}$$

The combinatorial optimization problem in (12) is intractable due to its high computational complexity. If the constraint $\boldsymbol{x} \in \{0,1\}^J$ is relaxed to $\boldsymbol{x} \in [0,1]^J$, we can obtain a more tractable and convex optimization problem as follows

$$\begin{aligned} \max_{\boldsymbol{x}} \quad & \lambda_2(\mathbf{L}'(\boldsymbol{x})) \\ \text{s. t.} \quad & \boldsymbol{x}^T\boldsymbol{y}_k \geq \mathcal{R}_k\gamma_{\text{th}}, \quad \forall k \in \{1,\ldots,K_m\}, \\ & \mathbf{1}^T\boldsymbol{x} = K_m, \ 0 \leq \boldsymbol{x} \leq 1. \end{aligned} \tag{13}$$

Proposition 2. *(13) is a convex optimization problem and can be reformulated as an equivalent semi-definite programming (SDP) optimization problem.*

Proof. Using (8), the Fiedler value of $\lambda_2(\mathbf{L}'(\boldsymbol{x}))$ can be expressed as $\lambda_2(\mathbf{L}'(\boldsymbol{x})) = \text{Inf}_{\boldsymbol{v}}\big\{\boldsymbol{v}^T\mathbf{L}'(\boldsymbol{x}))\boldsymbol{v}, \quad \|\boldsymbol{v}\|_2 = 1, \quad \mathbf{1}^T\boldsymbol{v} = 0\big\}$, which is the point-wise infimum of a family of linear functions of $\boldsymbol{x}$ [9]. Hence, $\lambda_2(\mathbf{L}'(\boldsymbol{x}))$ is a concave function in $\boldsymbol{x}$. Additionally, the constraints of (13) are linear in $\boldsymbol{x}$. Therefore, the optimization problem in (13) is a convex optimization problem, and it is equivalent to the following

TABLE I
SIMULATION PARAMETERS

Parameter	Value	Parameter	Value
K_m	2	h	200
c	3×10^8 m/s	f_c	3 GHz
P	30 dBm	p	23 dBm
β_0	10^{-6}	γ_0^{RIS}	60 dB
B	250 KHz	J	40
R^{RIS}	150 m	N_0	-120 dBm

SDP optimization problem [15], [16]

$$\max_{\mathbf{x},s} \quad s \tag{14}$$
$$\text{s. t.} \quad s(\mathbf{I} - \frac{1}{|\mathbf{x}|}\mathbf{1}\mathbf{1}^T) \preceq \mathbf{L}'(\mathbf{x}),$$
$$\boldsymbol{x}^T \boldsymbol{y}_k \geq \mathcal{R}_k \gamma_{\text{th}}, \quad \forall k \in \{1, \ldots, K_m\},$$
$$\mathbf{1}^T \boldsymbol{x} = K_m, \ 0 \leq \boldsymbol{x} \leq 1,$$

where $\mathbf{I} \in \mathbf{R}^{V \times V}$ is the identity matrix and $\mathbf{F} \preceq \mathbf{L}$ indicates that $\mathbf{L} - \mathbf{F}$ is a positive semi-definite matrix. ■

The optimization problem in (14) can be efficiently solved using standard SDP solvers, such as the CVX SDPT3 solver [17]. After solving, since the entries of output vector $\boldsymbol{x}$ are continuous, we select the top K_m largest values and set them to 1, while the remaining entries are set to 0.

V. NUMERICAL RESULTS

We consider a 3D scenario where the locations of UAVs are optimized, while the RIS and UE have fixed locations. However, the positions of the RIS and UE are updated in each simulation iteration. In these simulations, we employ the 3GPP Urban Micro (UMi) model [18] at a carrier frequency of 3 GHz to calculate all large-scale path loss values, consistent with the related works [19], [20]. Additionally, we assume a Nakagami$-f$ shape parameter of $f_1 = f_2 = 5$ for the cascaded UE-RIS-UAV link and $f = 1$ for the direct UE-UAV links, with a spread parameter of unity for all the links. Similar to [13], we use $\sqrt{\frac{\beta_0}{(d^{\text{UR}})^2}}$ and $\sqrt{\frac{\beta_0}{(d_k^{\text{RK}})^2}}$ for UE $\rightarrow$ RIS and RIS $\rightarrow$ UAV$_k$ links, respectively, where β_0 denotes the path loss at the reference distance $d_{\text{ref}} = 1$ m and d is the corresponding distance. The RIS is located at an altitude of 120 m. Other simulation parameters are given in Table I.

To evaluate the performance of the proposed scheme, we consider the scheme proposed in [14] that utilizes the whole RIS to create one link only and the original scheme without the RIS, inspired by [3]. Additionally, we consider the random scheme and the proposed scheme but without optimizing the UAVs locations.

First, we present some numerical results to assess the approximation of removing the non-aligned term in (2). We plot the exact rate in (2), while including the non-aligned term, and the approximated rate using (6). For the purpose of this part, the fixed 3D coordinates in meters for the UE are $(118, 220, 0)$, while UAV$_1$, UAV$_2$, and the RIS are located at $(160, 140, 200)$, $(170, 14, 200)$, and $(0, 0, 120)$, respectively. In

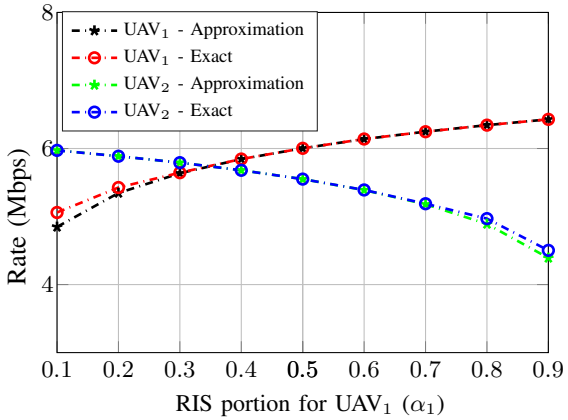

Fig. 3. Rate performance versus α_1.

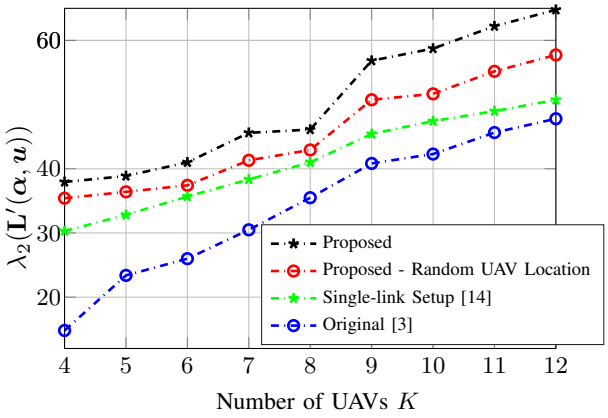

Fig. 4. Network connectivity versus K for a well-connected network with $\gamma_{\text{th}} = 60$ dB, $\gamma_0^{\text{UAV}} = 75$ dB, and $\gamma_0^{\text{UE}} = 70$ dB.

Fig. 3, the presented results are averaged over 10^5 simulations. For UAV$_1$ and UAV$_2$, the RIS partitions, respectively, are α_1 and $\alpha_2 = 1 - \alpha_1$. We adopt the phase shift quantization levels similar to [12]. From the figure, we notice that approximated rates for the UAVs tightly match the exact rates for most values of α_1. Overall, these results justify our assumption to (i) ignore the impact of non-aligned channels from the other portions of the RIS and (ii) approximate (2) by (6). Therefore, in the remaining of the figures, we will use the approximated SNR expression in (6). Additionally, the figure shows that as α_1 increases, more RIS elements are allocated to support the link to UAV$_1$. As a result, the exact and the approximated rates of UE $\xrightarrow{\text{RIS}}$ UAV$_1$ link increase, while both rates of UE $\xrightarrow{\text{RIS}}$ UAV$_2$ link decrease.

Next, we present the network connectivity results for two scenarios: a well-connected network and a sparse network, with 40 grid points for the UAVs K_m. In the well-connected scenario, we assume high connectivity among the UAVs and between the UE and the UAVs, meaning direct links between the UE and the UAV(s) are always present. In this case, the original network forms one connected graph (i.e., $\lambda_2(\mathbf{L}) = 0$), where no node is disconnected from the network. For this scenario, we set $\gamma_0^{\text{UAV}} = 75$ dB and $\gamma_0^{\text{UE}} = 70$ dB. The results are plotted in Fig. 4 as a function of the number of UAVs

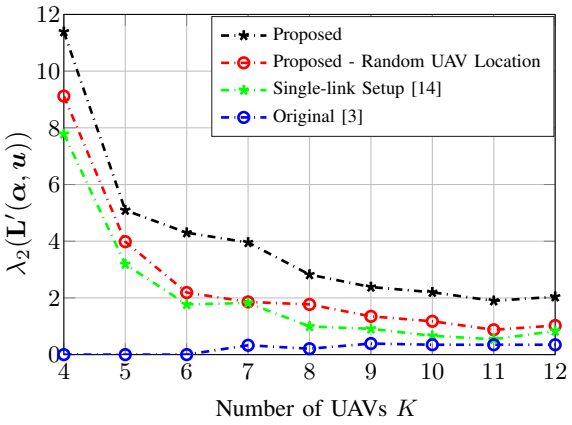

Fig. 5. Network connectivity versus K for a sparse network with $\gamma_{\text{th}} = 60$ dB and $\gamma_0^{\text{UAV}} = \gamma_0^{\text{UE}} = 83$ dB.

K. As shown, the proposed scheme consistently outperforms other schemes due to the joint optimization of RIS partitioning and UAV placement, which enables (i) the RIS to establish two potential links and (ii) optimal UAV positioning that improves the quality of these links. In contrast, the single-link setup shows noticeable degradation compared to the proposed scheme with random UAV placement, as it only creates one link from the RIS.

On the other hand, for the sparse network, we set $\gamma_0^{\text{UAV}} = \gamma_0^{\text{UE}} = 83$ dB. In this case, the original network is not always fully connected, occasionally resulting in zero connectivity. Therefore, the performance of the original scheme fluctuates between zero and positive values (i.e., > 0), but the presented results are averaged over 500 Monte Carlo simulations. The outcomes are plotted in Fig. 5 as a function of the number of UAVs K. Since the network is sparse due to the high SNR thresholds for the UE $\rightarrow$ UAV and UAV$_k$ $\rightarrow$ UAV$_{k'}$ links, adding more UAVs does not lead to increased connectivity as observed in Fig. 4. This is because deploying more UAVs, while many of their connections fail to meet the high SNR thresholds, results in a sparser network graph (i.e., more nodes but fewer edges). Consequently, the network connectivity of the RIS-assisted schemes decreases, in contrast to Fig. 4, where the network graph is highly connected and approaches a semi-complete graph structure.

VI. Conclusion

This work formulates and solves the network connectivity maximization problem, characterized by the Fiedler value, through a joint optimization of UAV positioning and RIS partitioning. With the assistance of RIS deployment and UAV positioning, we aim to enhance the network connectivity of uplink RIS-assisted UAV networks. Closed-form solution for RIS partitioning and SDP optimization for UAVs positioning are developed and benchmarked against several schemes, including original, random UAVs locations, and a single-link setup. Our simulations show that the effect of UAV positioning and RIS partitioning on the network connectivity is significant compared to these benchmark schemes.

References

[1] M. Z. Hassan, G. Kaddoum, and O. Akhrif, "Interference management in cellular-connected internet of drones networks with drone-pairing and uplink rate-splitting multiple access," *IEEE Internet of Things Journal*, vol. 9, no. 17, pp. 16 060–16 079, 2022.

[2] M. Saif, M. Z. Hassan, and M. J. Hossain, "Decentralized aggregation for energy-efficient federated learning in mmwave aerial-terrestrial integrated networks," *IEEE Transactions on Machine Learning in Communications and Networking*, pp. 1–1, 2024.

[3] M. A. Abdel-Malek, A. S. Ibrahim, and M. Mokhtar, "Optimum uav positioning for better coverage-connectivity tradeoff," in *2017 IEEE 28th Annual International Symposium on Personal, Indoor, and Mobile Radio Communications (PIMRC)*, 2017, pp. 1–5.

[4] M. Ammous and S. Valaee, "Cooperative positioning with the aid of reconfigurable intelligent surfaces and zero access points," in *2022 IEEE 96th Vehicular Technology Conference (VTC2022-Fall)*, 2022, pp. 1–5.

[5] A. Parchekani and S. Valaee, "Sensing and localization using reconfigurable intelligent surfaces and the Swendsen-Wang algorithm," in *2022 IEEE International Conference on Communications Workshops (ICC Workshops)*, 2022, pp. 981–986.

[6] M. Javad-Kalbasi, M. S. Al-Abiad, and S. Valaee, "Energy efficient communications in RIS-assisted UAV networks based on genetic algorithm," in *GLOBECOM 2023 - 2023 IEEE Global Communications Conference*, 2023, pp. 5901–5906.

[7] M. Obeed and A. Chaaban, "Joint beamforming design for multiuser MISO downlink aided by a reconfigurable intelligent surface and a relay," *IEEE Transactions on Wireless Communications*, vol. 21, no. 10, pp. 8216–8229, 2022.

[8] K. Weinberger, R.-J. Reifert, A. Sezgin, and E. Basar, "RIS-enhanced resilience in cell-free MIMO," in *WSA SCC 2023; 26th International ITG Workshop on Smart Antennas and 13th Conference on Systems, Communications, and Coding*, 2023, pp. 1–6.

[9] A. S. Ibrahim, K. G. Seddik, and K. R. Liu, "Connectivity-aware network maintenance and repair via relays deployment," *IEEE Transactions on Wireless Communications*, vol. 8, no. 1, pp. 356–366, 2009.

[10] C. Pandana and K. R. Liu, "Robust connectivity-aware energy-efficient routing for wireless sensor networks," *IEEE Transactions on Wireless Communications*, vol. 7, no. 10, pp. 3904–3916, 2008.

[11] M. Fiedler, "Algebraic connectivity of graphs," in *Czechoslovak Mathematical J.*, vol. 23, 1973, pp. 298–305.

[12] S. Arzykulov, A. Celik, G. Nauryzbayev, and A. M. Eltawil, "Aerial RIS-aided physical layer security: Optimal deployment and partitioning," *IEEE Transactions on Cognitive Communications and Networking*, pp. 1–1, 2024.

[13] M. S. Al-Abiad, M. Javad-Kalbasi, and S. Valaee, "Maximizing network connectivity for UAV communications via reconfigurable intelligent surfaces," in *GLOBECOM 2023 - 2023 IEEE Global Communications Conference*, 2023, pp. 6395–6400.

[14] ——, "Effectiveness of reconfigurable intelligent surfaces to enhance connectivity in UAV networks," 2023. [Online]. Available: https://arxiv.org/abs/2308.10788

[15] S. Boyd, "Convex optimization of graph laplacian eigenvalues," in *Proc. International Congress of Mathematicians,*, vol. 3, 2006, pp. 1311–1319.

[16] S. Boyd and L. Vandenberghe, "Convex optimization," in *Cambridge University Press,*, vol. 3, 2006, pp. 1311–1319.

[17] "SDPA-M package," in *[Online]. Available: http://grid.r.dendai.ac.jp/sdpa/.*

[18] K. Haneda, J. Zhang, L. Tan, G. Liu, Y. Zheng, H. Asplund, J. Li, Y. Wang, D. Steer, C. Li, T. Balercia, S. Lee, Y. Kim, A. Ghosh, T. Thomas, T. Nakamura, Y. Kakishima, T. Imai, H. Papadopoulos, T. S. Rappaport, G. R. MacCartney, M. K. Samimi, S. Sun, O. Koymen, S. Hur, J. Park, C. Zhang, E. Mellios, A. F. Molisch, S. S. Ghassamzadeh, and A. Ghosh, "5G 3GPP-like channel models for outdoor urban microcellular and macrocellular environments," in *2016 IEEE 83rd Vehicular Technology Conference (VTC Spring)*, 2016, pp. 1–7.

[19] E. Björnson, Özdogan, and E. G. Larsson, "Intelligent reflecting surface versus decode-and-forward: How large surfaces are needed to beat relaying?" *IEEE Wireless Communications Letters*, vol. 9, no. 2, pp. 244–248, 2020.

[20] J. Lyu and R. Zhang, "Spatial throughput characterization for intelligent reflecting surface aided multiuser system," *IEEE Wireless Communications Letters*, vol. 9, no. 6, pp. 834–838, 2020.